Motor engram as dynamic change of the cortical network during early sequence learning: an fMRI study

Hamano, Yuki H.

DOCTOR OF PHILOSOPHY

SOKENDAI (The Graduate University for Advanced Studies)

School of Life Science

Department of Physiological Sciences

Table of Contents

1. Summary

Practice improves the performance of skilled movements, both in speed and accuracy. Emphasis on speed improves performance by defining an optimal learning target, but learning can occur even without speed incentives. Little is known how these characteristics of the practice, the speed or accuracy, are integrated to form the neural substrates of the sequence learning, that is, engram.

An engram has four characteristics: persistence, ecphory, content, and dormancy. An engram is a persistent change in the brain by a specific experience or encoding. An engram is activated through interaction with retrieval cues, which activation is termed ecphory. The content of an engram reflects what transpired at encoding thus predicts what can be recovered during subsequent retrieval. An engram exists in a dormant state between the two active processes of encoding and retrieval. During dormant state, the strength of the synaptic connection is stabilized. At retrieval, the connections are destabilized so that the synaptic connections are modified. Thus, the series of the active states of encoding and retrieval intervened by dormant state comprises the learning process, resulting in the serial change in the spatiotemporal

pattern of the neural ensemble. The neural substrate of motor engrams in the human brain is hard to identify because their dormant state is hard to discriminate. The previous neuroimaging approaches to find out the motor engram have mainly focused on the ecphory.

Here I utilized eigenvector centrality (EC) as the measure of the information transfer at the network level accumulation, expecting that the trace of brain changes brought about by motor training--the motor engram--may be determined using functional MRI. EC is a class of graph theory-based measures assessing the centrality or importance. While the eigenvector centrality favors nodes that have high correlations with many other nodes, it specifically favors nodes that are connected to nodes that are themselves central within the network. Thus, the EC takes into account the entire pattern of the network, allowing us to estimate the importance of each voxel within the whole brain network with seed- and task-free fashion.

To discriminate the engrams formed by an emphasis on speed or accuracy targets, I conducted functional MRI with 58 normal volunteers, who performed a sequential finger tapping task with the non-dominant left hand inside the scanner.

Participants practiced a tapping sequence alternately as quickly as possible (maximum mode) or at a constant speed of 2 Hz, paced by a visual cue which specified the sequence (constant mode). My hypothesis was that different learning modes enhance distinct engrams. To quantify brain changes at the network level that characterize the engram, even when dormant, I applied the EC to the residual time-series after modeling out the task-related activity, because the residual BOLD (Blood-Oxygen-Level-Dependent) signals were thought to include task-non-specific neural fluctuations, corresponding to spontaneous brain activity.

The performance was transferred from the constant mode to maximum mode, but not vice versa. During the maximum mode, areas of greatest network centrality indicating the engram location were found in in the left anterior intraparietal sulcus (aIPS), connecting with the ventral inferior parietal lobule (IPL). During the constant mode, a distinct engram was found in bilateral dorsal premotor cortex and right primary motor cortex (M1). A learning-related increment in task-related activity in the right M1 was observed in both modes.

Learning-related enhancement of EC in the left aIPS during rest condition of the maximum mode probably represented the accumulation of information provided by the comparison between the action plan of the rapid transition of the one finger to the next in the sequence and the actual feedback. Thus, the left aIPS-IPL represented the sensorimotor integration of precisely tuned rapid finger movements the one finger to the next in the sequence. The PMd is a probable substrate for the coordinate transformation from the visually presented spatial goals to joint movements in the response domain through associative learning, coding the accuracy with the M1. Therefore, within an M1-centered parietal-premotor network motor engram, the left aIPS-IPL appears to represent the sensorimotor integration of precisely timed rapid finger movements, and the PMd and M1 the accuracy of their assignment. Present findings constitute the first demonstration of motor engrams formed by only 30 min of training.

2. INTRODUCTION

Practice is responsible for obtaining a motor skill which is characterized by

speed and accuracy (Shmuelof et al. 2012). The practice effect may differ depending on

whether stressing on the speed or accuracy. Speed pressure is known to enhance the

learning process. Motor learning is to establish an internal model which represents the

exact matching between perceived sensory and motor information (Wolpert et al.,

1995). Information is transmitted during learning by comparing the expected sensation

by the internal model with the actual feedback sensation arising from the movement

(Guadagnoli and Lee, 2004). So as to generate the information for the learning to occur,

task difficulty should be kept challenging. Speed can adjust a specific difficulty level of

the sequential finger tapping task (Walker et al., 2002, 2003; Fischer et al., 2002, 2005;

Debas et al., 2010). They usually requested the participants to practice the given

sequence "as fast and as accurately as possible." However, even without speed pressure,

sequence learning occurs by serial reaction time tasks (Doyon et al. 1996; Grafton et al.

1994; Hazeltine et al. 1997; Krebs et al. 1998; Rauch et al. 1997; Honda et al. 1998)

which stress on accuracy. Little is known how these characteristics of the practice, the

speed and accuracy, are integrated to form the neural substrates of the sequence

learning, that is, engram.

An engram has four characteristics: persistence, ecphory, content, and dormancy

(Josselyn et al. 2015). An engram is a persistent change in the brain by a specific

experience or encoding. An engram is activated through interaction with retrieval cues,

which activation is termed ecphory. The content of an engram reflects what transpired

at encoding thus predicts what can be recovered during subsequent retrieval. An engram

exists in a dormant state between the two active processes of encoding and retrieval.

During dormant state, the strength of the synaptic connection is stabilized. At retrieval,

the connections are destabilized so that the synaptic connections are modified. Thus the

series of the active states of encoding and retrieval intervened by dormant state

comprises the learning process, resulting in the serial change in the spatiotemporal

pattern of the neural ensemble (Josselyn et al. 2015).

Previous neuroimaging approaches to find out the motor engram have mainly

focused on the ecphory because they utilized task-related activation to evaluate the

effect of learning (Doyon et al. 2003; Penhune and Doyon, 2002; Lehéricy et al. 2005).

Regarding the dormant engram, recent resting-state fMRI studies before and after the

visuomotor learning task (Albert et al. 2009) have found learning-related change in

frontoparietal and cerebellar networks. However, it is unknown how these two states of

engram are dynamically represented in the neural network level.

To address this issue, I conducted functional MRI with sequential finger tapping

execution epoch alternated with rest epoch. I hypothesized that the two learning modes,

stressing on speed or accuracy, generate distinct engrams which in turn are integrated at

the execution. I focused on the early phase of training of 30 min.   Participants

exercised a sequence as fast and as accurate as possible (maximum mode) or with

constant speed by visual cues explicitly indicating the sequence (2 Hz, constant mode).

Participants alternated constant mode with the maximum mode. I applied eigenvector

centrality mapping (ECM; Lohmann et al., 2010) to the innovation. Eigenvector

Centrality (EC) is a class of graph theory-based measures assessing the centrality or

importance (Zuo et al. 2012). Innovation is the residual time-courses of the neural

activities obtained by modeling out the task-related effects and other confounding

effects. The innovation of BOLD signals is thought to include task-non-specific neural

fluctuations, corresponding to spontaneous brain activity (Fox et al. 2007; Riera et al.

2004; Fair et al. 2007). Regarding the innovation, I made a distinction between the task

epoch in which encoding/retrieval occurred and the rest epoch which was in a dormant

state. I expected that the M1 centered cortical network would represent the motor

engram.

3. Materials and methods

3.1 Participants

A total of 60 healthy right-handed normal adult volunteers participated in the study. Handedness was assessed by the Edinburgh Handedness Inventory (Oldfield, 1971). None of the participants had a history of neurological or psychiatric diseases. All participants gave written informed consent for participating the experiment, and the study was conducted according to the Declaration of Helsinki and approved by the Ethical Committee of the National Institute for Physiological Sciences, Japan. Data obtained from two volunteers were of insufficient quality (button pressing in wrong timing for 1 participant, and the measurement failure in another). Therefore, data from 58 individuals (34 males and 24 females; mean age = 21.69 ± 3.88 years) were analyzed.

3.2 Task

The subjects performed sequential finger tapping task (Walker et al., 2002, 2003) inside the scanner with two modes: a visually-cued (2Hz) constant mode and

maximum mode. Presentation 12.2 software (Neurobehavioral Systems, Albany, USA) was implemented on a personal computer (dc7900; Hewlett-Packard, Ltd., Palo Alto, USA) for the stimulus presentation and response time measurements. A liquid-crystal display (LCD) projector (CP-SX12000J, Hitachi Ltd., Tokyo, Japan), located outside and behind the scanner, projected stimuli through another waveguide to a translucent screen that the participants viewed via a mirror attached to the head coil of the MRI scanner. The distance between the screen and each participant's eyes was approximately 175 cm, and the visual angle was 13.8° (horizontal) × 10.4° (vertical).

There were three fMRI runs. First run (Run 1) consisted of a block of constant-speed mode (C block) followed by a block of maximum mode (M block). C block (Figure 1), 2.5 min in duration, started with Rest epoch of 15 sec duration followed by Constant mode epoch of 15 sec, alternatively repeated five times. Rest epoch started with the instruction of "Rest" on the screen for 500 ms, followed by 500 ms presentation of four blue filled circles aligned within an equally spaced horizontal array, corresponding to the left-hand fingers (from left to right, small, ring, middle, and index fingers) (Figure 1). The instruction was to follow the randomly moving blue

circles of 2 Hz with eyes without pressing the button. Rest epoch lasted for 15 sec when

the target "CONSTANT" appeared to instruct the participant to respond by pressing the

button indicated by white filled circle. The visual cues were identical to those of Rest

epoch except for the color and sequence of lighting (Figure 1). One of the circles was

filled in every 500 ms, indicating the tapping fingers and buttons on an MR-compatible

button box (Current Design, Inc., Philadelphia, USA). A sequence was composed of the

five element sequences, either "index – little – middle – ring - index" (presented to 31

participants) or "ring – middle – little – ring - index" (presented to other 27

participants). The frequency of the color and location change was kept 2 Hz. Constant

epoch lasted 15 sec when alternated with Rest epoch. Rest and Constant epochs were

conducted alternatively five times, constituting the C block 1. M block 1 (Figure 1), 3

min in duration, started with Rest epoch which was identical to that of C block except

for its duration of 30 sec instead of 15 sec. Instruction of "TEST" was shown for 500

ms to ask the participant to tap the memorized sequence as fast and as accurate as

possible, and four closed white circles were presented for 500 ms when they changed to

open circles. Visual feedback of correct tapping was provided by the filling of the white

circle corresponding to the tapped finger. If the participant made an incorrect response,

the stimulus remained at the previous visual cue until the correct button was pressed.

Maximum epoch lasted 30 sec. Rest and Maximum epochs were conducted alternatively

three times.

The second Run (Run 2) consisted of 3 C blocks interleaved by 2 M blocks,

and the third Run (Run 3) started with M block followed by C block. Overall, the

sequential finger task in this study was built with 5 C blocks (a total of 12.5 min) and 4

M blocks (12 min) alternate (Figure 1). By interleaving two modes alternately, the

learning effect by the constant-speed mode was able to be evaluated by measuring speed

and accuracy during maximum speed mode (See the following section in detail).

3.3 Behavior analysis

The performance was measured by speed, accuracy, and "performance index"

by combining transition time (*TT*) and error rate (*ER*) (Equation 1; modified from Dan

et al., 2015), taking into account of speed-accuracy trade-off (Fitts, 1954). Transition

time (in seconds) was defined by the mean time between two correct button responses

per block. The error rate was the number of error responses about all responses per

block.

Equation 1: $PI = exp^{-TT} \times exp^{-ER} \times 100$

Because the behavioral task consisted of several blocks including three or five

epochs (Figure 1), I dissociated the between-block effect and within-block effect for the

performance changes in both constant-speed and maximum-speed modes. For each

performance measures (i.e., transition time, error rate, and performance index) and each

mode (constant and maximum), a repeated measure analysis of variance (rmANOVA)

was conducted with task epoch and task block as the independent variable. Bonferroni

correction was adopted for posthoc multiple comparisons. All statistical analyses were

performed by SYSTAT (version 13.00.05, SYSTAT Software, USA) and the level of

significance was $p < .05$.

3.4 fMRI scanning parameters

A 3.0T scanner (Verio; Siemens Ltd., Erlangen, Germany) was used for the

fMRI study. Each participant's head was immobilized within a 32-element phased array

head coil. fMRI was performed using a multiband GE-EPI sequence (Moeller et al.,

2009; echo time [TE] = 30 ms, repetition time [TR] = 1,000 ms; field of view [FOV] =

192×192 mm^2; flip angle = 80°; matrix size = 96×96; 60 slices; slice thickness = 2 mm;

multiband factor = 8). A whole-brain high-resolution T1-weighted anatomical

magnetization-prepared rapid-acquisition gradient echo (MP-RAGE) MRI was also

acquired for each participant (TE = 2.97 ms; TR = 1,800 ms; FOV = 256×256 mm^2; flip

angle = 9°; matrix size = 256×256; slice thickness = 1mm).

3.5 fMRI data processing

Image processing and statistical analyses were performed using the Statistical

Parametric Mapping (SPM12) package (http://www.fil.ion.ucl.ac.uk/spm/). The first

five volumes of each fMRI run were discarded to allow the MR signal to reach a state of

equilibrium. The remaining volumes were used for the subsequent analyses. To correct

for subject's head motion, functional images from each run were realigned to the first

image and again realigned to the mean image after the first realignment. The T1-

weighted anatomical image was coregistered to the mean of all realigned images. Each

coregistered T1-weighted anatomical image was normalized to the MNI space with the

DARTEL procedure (Ashburner, 2007). More specifically, each anatomical image was

segmented into the tissue class images using a unified segmentation approach

(Ashburner and Friston, 2005). The gray and white matter images were transformed to a

common coordinate space using the DARTEL registration algorithm. I used the

institute-specific template, which was created from study-independent 530 individuals

(150 females; Tanabe et al., 2014), to estimate the parameters in the DARTEL

registration. The parameters from the DARTEL registration and normalization to MNI

space were then applied to each functional image. The normalized functional images

were filtered using a Gaussian kernel of 5 mm FWHM in the x, y, and Z-axes.

3.6 fMRI data analysis

A general linear model was fitted to the fMRI data for each participant

(Friston et al., 1994; Worsley and Friston, 1995, Figure 2). The time series of the BOLD

signal was modeled with boxcar functions corresponding to each and all task epoch

convolved with the canonical hemodynamic response function. The first and third runs

included eight task-related regressors, five for tapping epochs in constant-speed and

three for those in maximum mode. The second run included 21 task-related regressors,

fifteen for tapping epochs in constant-speed mode and six for those in maximum mode.

The time series for each voxel was high-pass filtered at 1/128 Hz. With a first-order

autoregressive model, the serial autocorrelation was estimated from the pooled active

voxels with the restricted maximum likelihood procedure and was used to whiten the

data (Friston et al., 2002). Motion-related artifacts were minimized by incorporating the

six parameters from the rigid-body realignment stage into each model. One additional

regressor, describing intensities in CSF compartments, was added to the model. The

estimates for each task-related regressor were evaluated using linear contrasts.

The parameter estimates for each regressor in each ("contrast" images) were

submitted to second level analysis (Holmes and Friston, 1998) with a flexible-factorial

model incorporated within-participant factors of 'Repetition' and 'Mode' (constant-

speed/maximum-speed). Pre-defined linear increasing and decreasing contrasts for each

mode were applied to depict the changes of task-related activity related to the learning

of a sequential finger-tapping skill. Increasing or decreasing contrast vector was defined

as numbers in increment or decrement of one per epoch with keeping mean to zero. The

resulting set of voxel values for each contrast constituted the SPM$\{t\}$, which was

transformed into normal distribution units (SPM$\{z\}$). The statistical threshold for the

spatial extent test on the clusters, which was defined by the height threshold of z = 3.09,

was set at $p < 0.05$ corrected for family-wise error (Friston et al., 1996)

3.7 Functional connectivity analysis

To explore the neuronal representation of the dormant motor engram during

constant mode and maximum mode, the model-free eigenvector centrality mapping was

adopted. Postulating dormant motor engram exists while motor execution was not

performed, I calculated eigenvector centrality within the residual time series of rest

epochs in each block. Considering that the functional connectivity pattern depends on

participants' state (Biswal et al., 1995), the residual time-series were divided into task

and rest epochs during the constant-speed mode and then concatenated each five epochs

data into one time-series data. Because the training task included 25 task epochs of

constant-speed mode and 25 rest epochs, the resulted concatenated residual time-series

were five task-state and five rest-state data. The same procedure was applied to the

maximum mode, generating four task-state and four rest-state data (Figure 2).

I applied eigenvector centrality mapping (ECM; Lohmann et al., 2010) to the

concatenated residual time-series. Utilizing the same gray matter mask defined by

averaging the segmented and DARTEL-normalized gray matter images from all

participants, ECM was conducted using LIPSIA package (Lohmann et al., 2010)

installed in PC with Debian Linux OS. I confirmed that the gray matter mask included

the cerebellum and the striatum. Let A be an n x n similarity matrix where entries a_{ij}, i,

j~1, …n contain a pairwise correlation coefficient between time series in voxels i and j,

n is the number of voxels within the gray matter mask. The matrix A is symmetric so

that each voxel can be viewed as a node in an undirected weighted graph in which

correlation coefficients correspond to weights along the edges of the graph. In graph-

based applications, these weights represent distances between nodes. In this study, I

utilized correlation matrix of the gray matter voxels in the whole brain, replacing the

negative correlation with zero. The eigenvector centrality x_i of node i is defined as the

ith entry in the normalized eigenvector x belonging to the largest eigenvalue of A (λ),

$$Ax = \lambda x$$
$$x = \frac{1}{\lambda} Ax$$
$$x_i = \mu \sum_j a_{ij} x_j$$

While the eigenvector centrality favors nodes that have high correlations with many

other nodes, it specifically favors nodes that are connected to nodes that are themselves

central within the network. Thus the eigenvector centrality takes into account the entire

pattern of the network (Lohman et al. 2010), allowing us to estimate the importance of

each voxel within the whole brain network with seed- and task-free fashion (Zuo et al.

2012).

To confirm that the centrality values obey a Gaussian normal distribution as

required for subsequent statistical tests, the estimated centrality maps were transformed

according to a previous study (van Albada et al., 2007). Subsequent statistical tests for

ECM was conducted in SPM12. The resulting gaussianized centrality maps for five

task-states and five rest-states in each participant were submitted to second level

analysis with a flexible-factorial model incorporated within-participant factors of

'Repetition' and 'State.' Similar to task-related activity, pre-defined linear increasing

contrasts for rest state was applied to depict the learning related network changes which

are state-dependent. Furthermore, to depict the retrieval related change in the network,

task state EC was compared with rest state EC. The statistical threshold for the spatial

extent test on the clusters, which was defined by the height threshold of z = 3.09, was

set at $p < 0.05$ corrected for family-wise error (Friston et al., 1996). An identical

analysis was applied to the maximum mode data.

3.8 Anatomical labeling and Visualization

Brain regions were anatomically defined and labeled according to the co-planer

stereotaxic atlas of the human brain (Mai et al. 2016). The MRIcron

(http://www.mccauslandcenter.sc.edu/mricro/mricron/)

was used to display activation patterns on T1- weighted MRI image.

4. Results

4.1 Behavioral results

To evaluate the between-block and within-block changes of behavioral performance with the acquisition of sequential finger tapping skill, I compared the PI between blocks and epochs in both constant and maximum modes, respectively. In the maximum mode, the block effect (Two-way multivariate repeated measures ANOVA, $F(3,55) = 11.21$, $p < 0.001$) and block x epoch interaction $F(6,52) = 5.129$ $p < 0.001$) were significant, while within-block effect was not significant ($F(3, 55) = 0.118$, $p = .889$) (Figure 3). To evaluate the transfer of the learning through the constant mode, I compared the PI of the last epoch of the preceding block with that of the first epoch of the following block. One way multivariate repeated measures ANOVA showed the significant main effect ($F(2, 56) = 3.4$, $p = 0.04$). The increment of the PI of the second from the first block was 1.75 +/- 3.12 (mean +/- SD, One-sample t-test, $t(57) = 4.28$, $p <0.001$, Bonferroni corrected), third and second was 0.55 +/- 2.00 ($t(57) = 2.07$, $p = 0.043$, uncorrected, Bonferroni corrected $P = 0.128$), and the fourth and third was 1.44 +/- 2.53 ($t(57) = 4.33$, $p < 0.001$, Bonferroni corrected) (Figure 4).

In the constant mode, learning related change of response time and its

standard deviation were evaluated with 57 participants out of 58, because of the

measurement failure.   No effect of the PI was shown in the constant-speed mode

(between effect: $F(4,228) = 1.09$, $p = .35$; within effect: $F(4,228) = 1.29$, $p = .28$;

interaction effect: $F(16,912) = .97$, $p = .47$) (not shown in Figure). For response time,

the block effect (Two-way repeated measures ANOVA, $F(4, 53) = 12.77$, $p < 0.001$),

epoch effect ($F(4, 53)=9.19$, $p < 0.001$), and their interaction ($F(16, 41) =7.36$, $p <$

0.001) were significant (Figure 3). The transfer effect from the preceding maximum

mode was not significant (repeated measures ANOVA, $F(3, 54) = 0.701$, $p = 0.556$)

(Figure 4). For the variability of the response time in terms of the standard deviation,

the block effect (Two-way repeated measures ANOVA, $F(4, 53)=1.595$, $p = 0.189$),

epoch effect ($F(4, 53)=2.338$, $p = 0.067$), or their interaction ($F(16, 41) =1.525$, $p =$

0.137) were not significant (Figure 3). The variability did not show transfer effect from

the preceding maximum mode (repeated measures ANOVA, $F(3, 54) = 1.085$, $p =$

0.363) (Figure 4). These findings indicated that both maximum and constant modes

enhanced the performance. Transfer of the learning was observed from constant mode

to maximum mode, but not in the reverse direction.

To further dissect the performance transfer from the constant mode to the

maximum mode, the transition time and error rate during the maximum mode was

evaluated (Figure 5). Transition time showed significant effect of block (rmANOVA,

$F(3, 55) = 48.261, P < 0.001$), epoch ($F(2, 56) = 37.998, P < 0.001$), and their interaction

($F(6, 52) = 7.011, P < 0.001$). Error rate showed significant effect of block (rmANOVA,

$F(3, 55) = 2.831, P = 0.047$) and epoch ($F(2, 56) = 26.223, P < 0.001$), but no significant

effect was found in their interaction ($F(6, 52) = 1.613, P = 0.162$). The transfer effect

from the preceding maximum mode was not significant in the transition time

(rmANOVA, $F(2, 56) = 2.273, p = 0.112$), nor error rate (rmANOVA, $F(2, 56) = 0.971, p$

$= 0.385$) (Figure 5 bottom).

4.2 Eigenvector centrality mapping

During the maximum mode, EC during rest significantly increased in the left

anterior interior parietal sulcus (aIPS) as learning proceeded, which EC was enhanced

by task execution (Figure 6). The seed-based analysis across the whole brain revealed

that the functional connectivity with aIPS was enhanced only in the left IPL as learning

proceeded (Figure 7).   As sequential motor learning proceeded, the centrality during

rest-state of the constant mode significantly increased in bilateral dorsal premotor cortex

and the right primary motor cortex (M1) which EC was enhanced by task execution

(Figure 8).

4.3 Task-related activity

During constant mode, the linear increments of task-related activity were

observed in the right M1. The right M1 also showed the same learning related increment

during the maximum mode. (Figure 9).

5. Discussion

5.1 Behavior

Behavioral results showed that both maximum and constant modes induced learning.

Maximum mode stressed the speed whereas constant mode requires the correct button

press prompted by the slow and constant frequency visual signals. Thus constancy and

accuracy were stressed. To compensate the speed-accuracy tradeoff, PI was calculated.

With this measure, the learning during maximum mode was enhanced by the preceding

constant mode, thus the constant mode training effect was transferred to the following

maximum mode performance. During constant mode, the reaction time decreased as

learning proceeded to reach the range of 150 ms, indicating the progress of the sequence

learning. The RT was not influenced by the preceding maximum mode, indicating no

transfer effect from maximum mode.

5.2 EC as the measure of a neuronal ensemble of the engram

I characterized the motor engram as the dynamic change during learning. First, I

repeated the practice intervened by the rest epochs to introduce the active state followed

by the dormant state latter of which was characterized by the enhanced EC as learning

proceeded. This characterization is based on the prevailing view that the formation of

engram involves the strengthening of synaptic connections leading to the formation of a

neuronal ensemble at multiple levels up to regional connections (Josselyn et al. 2015).

As engram is to be enhanced by the retrieval (ecphory), EC of the dormant engram

should be enhanced during the task. Enhanced EC of the region indicated the enhanced

functional connectivity of the particular location with other regions, confirming that the

region is the part of the activated ensemble, that is, the ecphory. Based on these

inferences, I conducted the conjunction analysis with the linear increase in the EC

during the rest epoch and its task related increase. By applying this method to different

learning modes, I successfully depicted the learning-mode specific engram formation.

5.3 Learning related enhancement of EC

Maximum mode

During the maximum mode, EC during rest significantly increased in the left aIPS as

learning proceeded, which EC was enhanced by task execution. In humans, aIPS

mediates the processing of sensorimotor integration of precisely tuned finger

movements (Binkofski et al. 1998). Seed-based functional connectivity analysis on the

resting epoch of the maximum blocks showed that the connectivity between left aIPS

and IPL was enhanced as learning proceeded. The ventral part of the IPL might be a

human homolog of the area PF/PFG complex (Hattori et al., 2008). Area PF extending

to the lower bank of the IPS and ventral area 6 are anatomically connected (Petrides and

Pandya, 1984; Matelli et al., 1986; Rizzolatti et al., 1998) to from several frontoparietal

circuits (Geyer et al., 2000). The IPL is also related to the integration of somatosensory

and visual information (Caminiti et al., 1996; Rizzolatti et al., 1997; for a review see

Wise et al., 1997). The parietal lesion, particularly on the left side, is implicated in

apraxia, disability to execute previously learned movements (Halsband and Lange 2006;

Wheaton and Hallett, 2007; Halsband et al. 2001). Halsband et al. (2001) found that the

apraxic patients with left parietal lesion showed most pronounced impairment in

learning actions which are referred to their body. They argued that the left parietal

cortex is related to the storage of information related to the body reference frame

(Halsband and Lange 2006). This notion was supported by the recent functional MRI

study by Verstynen et al. (2014) In the present study, learning-related enhancement of

EC in the left aIPS during rest condition of the maximum mode probably represented

the accumulation of information provided by the comparison between the action plan of

the rapid transition of the one finger to the next in the sequence and the actual feedback.

Constant mode

During constant mode, engram was generated in the bilateral PMd and right

M1. As the task of the constant mode was the slow, visually guided finger tapping of the

predefined sequence, there was no need to retrieve the sequence per se, without speed

pressure. However, translation of the extrinsically defined goals into muscle coordinates

was required (Wiestler et al. 2014). There was no performance transfer from the

preceding maximum mode. Still, the performance measured by RT improved. Thus the

participants have learned at least the sequence of stimulus-response relationship. The

performance was transferred to the subsequent maximum mode. Thus the engram

during the constant mode should represent the learning results accessible to the

maximum mode, that is, the sequence in the response domain (Keele et al. 1995).

PMd

The PMd is the dorsolateral subdivision of BA 6, defined as the agranular frontal cortex situated between the primary motor cortex (M1) and the prefrontal cortex. Recently, Genon et al. (2017) divided the right PMd into five subregions using the connectivity-based parcellations with resting state fMRI and probabilistic diffusion tractography. The present cluster on the right is corresponding to the central to the caudal subregions extending to the right M1. According to Genon et al. (2017), the central PMd is more tightly connected to the IPS and the SPL than other subregions which were functionally coupled to the central PMd. The central PMd is related to both motor and cognitive functions such as action execution and working memory, whereas the caudal PMd is related to motor preparation and programming, corresponding to nonhuman primate's caudal right PMd (area F2) (Geyer et al. 2000; Abe and Hanakawa 2009).

Clinically lesions of the premotor cortex were characterized by the disintegration of the dynamics of the motor act and skilled movements such as smooth typewriting or piano playing (Kleist, 1907, 1911; Luria, 1966). Previous non-human

primate study (Hoshi and Tanji 2006) showed that PMd neurons were able to retain and

combine the information of spatial target and effector to generate information

specifying a forthcoming action. Utilizing multivariate pattern analysis on the fMRI

data of the sequential finger tapping learning of both hands, Wiestler et al. (2014)

showed that the PMd represented the extrinsic (world-centered) sequence

representation. On the other hand, the primary sensory and motor cortices showed

representation in intrinsic (body-centered) space, with considerable overlap of the two

reference frames in the caudal PMd, showing a gradual transition between coding in

extrinsic and intrinsic coordinate frames. Therefore PMd is a probable substrate for the

coordinate transformation from spatial goals to joint movements through associative

learning (Kantak et al. 2016) between arbitrary, yet behaviorally relevant cues and

appropriate motor commands (stimulus-response relationship) and its conversion to the

response domain (Keele et al. 1995).

M1

I found the motor engram formation in the right M1 during the constant mode.

The M1 is known to play a role in procedural motor learning (Pascual-Leone and

Torres, 1993; Pascual-Leone et al. 1993, 1995; Karni et al. 1995; Honda et al. 1998;

Muellbacher et al., 2002; Lu & Ashe, 2007). Recent neuroimaging study showed that

contralateral M1 integrated the spatial and temporal information of learned finger

sequences encoded separately in the premotor cortex (Kornysheva & Diedrichsen,

2014), suggesting the integrating functions of the right M1 for the execution.

5.4 Learning related change of task-related activation

In the present study, I made the conjunction analysis regarding the learning

related increment of the task-related activation with different modes. I found that both

maximum and constant modes enhanced the task-related activation of the right M1 as

the learning proceeded. During constant speed mode, given the performance effect was

constant, the execution-related activation increment of the right M1 probably

represented the ecphoric process, consistent with the previous study (Hazeltine et al.

1997). The previous studies with maximum mode concluded the explicit motor learning-

related increase in the M1 are likely representing the velocity effect (Halsband and

Lange, 2006; Orban et al. 2010), because the task-related activation of M1 depends on

the speed (Jancke et al. 1998; Sadato et al. 1996, 1997) and force (Dettmers et al. 1995).

However, considering that the learning transfer was observed only from the constant

mode to maximum mode, not vice versa, and, that the right M1 is the only common area

showing the task-related learning effect where the engram of the constant mode learning

was represented, the maximum mode may take advantage of the preceding engram

formation in the right M1 by the constant mode. Considering the constant mode did

stress the constant response to the visual cue but not the speed, the learned engram in the

right M1 by the constant mode probably encode the accuracy which was transferred to

the speed-stressed maximum mode performance.

Distinct engram formation in the parietal and premotor regions and the

integrative process at the M1 are consistent with the notion that the praxis preparation

and execution are represented by the parietal and premotor areas (Johnson-Frey et al.

2005; Fridman et al. 2006; Wheaton et al. 2005). Wheaton and Hallett (2007) postulated

that the parietal cortex stores the concept of the movements and the premotor cortex

modifies the concept to a specific motor plan for motor cortex implementation.

6. Conclusion

In conclusion, the motor engram of the sequential finger tapping is formed in the M1-

centered parietal-premotor network, which is recruited by the M1 during the task

performance.

7. Acknoledgement

Firstly, I would like to express my sincere gratitude to my advisor Prof. Norihiro Sadato for the continuous support of my Ph.D study and related research, for his patience, motivation, and immense knowledge. His guidance helped me in all the time of research and writing of this thesis.

My sincere gratitude goes to Dr. Sho K. Sugawara and Dr. Masaki Fukunaga for providing me an opportunity to join the team and encouraging me with all the support and assistances throughout my experiment and past these 5 years of my Ph.D course. I would like to thank to other laboratory members who helped and made my experiment successful.

Besides my laboratory members, my special appreciation goes to Dr. Robert Turner for advising and encouraging me with his all the knowledge, research ideas and passion.

Last but not the least, I would like to thank my family: my parents and my brothers for supporting me spiritually throughout writing this thesis and my life in general. Words cannot be expressed enough.

8. References

Abe M, Hanakawa T (2009) Functional coupling underlying motor and cognitive functions of the dorsal premotor cortex. Behav Brain Res 198:13–23.

Albert NB, Robertson EM, Miall RC (2009) The resting human brain and motor Learning. Curr Biol 19:1023–1027.

Ashburner J (2007) A fast diffeomorphic image registration algorithm. Neuroimage 38:95–113.

Ashburner J, Friston KJ (2005) Unified segmentation. Neuroimage 26:839–851.

Binkofski F, Dohle C, Posse S, Stephan KM, Hefter H, Seitz RJ, Freund HJ (1998) Human anterior intraparietal area subserves prehension: A combined lesion and functional MRI activation study. Neurology 50:1253–1259.

Biswal B, Yetkin FZ, Haughton VM, Hyde JS (1995) Functional connectivity in the motor cortex of resting human brain using echo-planar MRI. Magn Reson Med 34:537–541.

Caminiti R, Ferraina S, Johnson PB (1996) The sources of visual information to the

primate frontal lobe: a novel role for the superior parietal lobule. Cereb Cortex

6:319–328.

Dan X, King BR, Doyon J, Chan P (2015) Motor Sequence Learning and Consolidation

in Unilateral De Novo Patients with Parkinson's Disease. PLoS One 10:e0134291.

Debas K, Carrier J, Orban P, Barakat M, Lungu O, Vandewalle G, Hadj Tahar A, Bellec

P, Karni A, Ungerleider LG, Benali H, Doyon J, Ungerleider (2010) Brain

plasticity related to the consolidation of motor sequence learning and motor

adaptation. Proc Natl Acad Sci USA 107:17839–17844.

Dettmers C, Fink GR, Lemon RN, Stephan KM, Passingham RE, Silbersweig D,

Holmes A, Ridding MC, Brooks DJ, Frackowiak RS (1995) Relation between

cerebral activity and force in the motor areas of the human brain. J Neurophysiol

74:802–815.

Doyon J, Owen A, Petrides M, Sziklas V, Evans A (1996) Functional anatomy of

visuomotor skill learning in human subjects examined with positron emission

tomography. Eur J Neurosci 8:637–648.

Doyon J, Penhune V, Ungerleider LG (2003) Distinct contribution of the cortico-striatal

and cortico-cerebellar systems to motor skill learning. Neuropsychologia 41:252–

262.

Fair DA, Schlaggar BL, Cohen AL, Miezin FM, Dosenbach NU, Wenger KK, Fox MD,

Snyder AZ, Raichle ME, Petersen SE (2007) A method for using blocked and

event-related fMRI data to study "resting state" functional connectivity.

Neuroimage 35:396–405.

Fischer S, Hallschmid M, Elsner AL, Born J (2002) Sleep forms memory for finger

skills. Proc Natl Acad Sci USA 99:11987–11991.

Fischer S, Nitschke MF, Melchert UH, Erdmann C, Born J (2005) Motor memory

consolidation in sleep shapes more effective neuronal representations. J Neurosci

25:11248–11255.

Fitts, P.M. 1954. The information capacity of the human motor system in controlling the amplitude of movement. *J. Exp. Psychol.* 67: 262-269.

Fox MD, Snyder AZ, Vincent JL, Raichle ME (2007) Intrinsic fluctuations within cortical systems account for intertrial variability in human behavior. Neuron 56:171–184.

Fridman EA, Immisch I, Hanakawa T, Bohlhalter S, Waldvogel D, Kansaku K, Wheaton L, Wu T, Hallett M (2006) The role of the dorsal stream for gesture production. Neuroimage 29:417–428.

Friston KJ, Holmes A, Poline J, Price CJ (1996) Detecting Activations in PET and fMRI : Levels of Inference and Power. Neuroimage 235:223–235.

Friston KJ, Jezzard P, Turner R (1994) Analysis of functional MRI time-series. Hum Brain Mapp 1:153–171.

Friston KJ, Penny W, Phillips C, Kiebel S, Hinton G, Ashburner J (2002) Classical and Bayesian Inference in Neuroimaging: Theory. Neuroimage 16:465–483.

Genon S, Li H, Fan L, Müller VI, Cieslik EC, Hoffstaedter F, Reid AT, Langner R,

Grefkes C, Fox PT, Moebus S, Caspers S, Amunts K, Jiang T, Eickhoff SB (2017)

The Right Dorsal Premotor Mosaic: Organization, Functions, and Connectivity.

Cereb Cortex 27:2095–2110.

Geyer S, Matelli M, Luppino G, Zilles K (2000) Functional neuroanatomy of the

primate isocortical motor system. Anat Embryol 202:443–474.

Grafton S, Woods R, Tyszka M (1994) Functional imaging of procedural motor

learning: relating cerebral blood flow with individual subject performance. Hum

Brain Map 1:221–234.

Guadagnoli MA, Lee TD (2004) Challenge point: a framework for conceptualizing the

effects of various practice conditions in motor learning. J Mot Behav 36:212–224.

Halsband U, Lange RK (2006) Motor learning in man: a review of functional and

clinical studies. J Physiol Paris 99:414–424.

Halsband U, Schmitt J, Weyers M, Binkofski F, Grützner G, Freund HJ (2001)

Recognition and imitation of pantomimed motor acts after unilateral parietal and

premotor lesions: A perspective on apraxia. Neuropsychologia 39:200–216.

Hattori N, Shibasaki H, Wheaton L, Wu T, Matsuhashi M, Hallett M (2009) Discrete

parieto-frontal functional connectivity related to grasping. J Neurophysiol

101:1267–1282.

Hazeltine E, Grafton ST, Ivry R (1997) Attention and stimulus characteristics determine

the locus of motor- sequence encoding. A PET study. Brain 120:123–140.

Holmes A, Friston KJ (1998) Generalisability, Random Effects & Population Inference.

Neuroimage 7:S745.

Honda M, Deiber MP, Ibanez V, Pascual-Leone A, Zhuang P, Hallett M (1998)

Dynamic cortical involvement in implicit and explicit motor sequence learning. A

PET study. Brain 121:2159–2173.

Hoshi E, Tanji J (2006) Differential involvement of neurons in the dorsal and ventral

premotor cortex during processing of visual signals for action planning. J

Neurophysiol 95:3596–3616.

Jancke L, Peters M, Schlaug G, Posse S, Steinmetz H, Muller-Gartner H (1998)

Differential magnetic resonance signal change in human sensorimotor cortex to

finger movements of different rate of the dominant and subdominant hand. Brain

Res Cogn Brain Res 6:279–284.

Johnson-Frey SH, Newman-Norlund R, Grafton ST (2005) A distributed left

hemisphere network active during planning of everyday tool use skills. Cereb

Cortex 15:681–695.

Josselyn SA, Köhler S, Frankland PW (2015) Finding the engram. Nat Rev Neurosci

16:521–534.

Kantak SS, Stinear JW, Buch ER, Cohen LG (2012) Rewiring the Brain. Neurorehabil

Neural Repair 26:282–292.

Keele SW, Jennings P, Jones S, Caulton D, Cohen A (1995) On the Modularity of

Sequence Representation. J Mot Behav 27:17–30.

Kleist K (1907) Corticale (innervatorische) apraxie. Jahrb Psychiatr Neurol 28:46–112.

Kleist K (1911) Der gang und der gegenwartige stand der apraxie-forschung.

Ergebnisse Neurol Psychiatr 1:342–452.

Kornysheva K, Diedrichsen J (2014) Human premotor areas parse sequences into their

spatial and temporal features. Elife 3:1–23.

Krebs HI, Brashers-Krug T, Rauch SL, Savage CR, Hogan N, Rubin RH, Fischman a J,

Alpert NM (1998) Robot-aided functional imaging: application to a motor learning

study. Hum Brain Mapp 6:59–72.

Lehéricy S, Benali H, Van de Moortele P-F, Pélégrini-Issac M, Waechter T, Ugurbil K,

Doyon J (2005) Distinct basal ganglia territories are engaged in early and advanced

motor sequence learning. Proc Natl Acad Sci USA 102:12566–12571.

Lohmann G, Margulies DS, Horstmann A, Pleger B, Lepsien J, Goldhahn D, Schloegl
H, Stumvoll M, Villringer A, Turner R (2010) Eigenvector centrality mapping for
analyzing connectivity patterns in fMRI data of the human brain. PLoS One
5:e10232.

Lu X, Ashe J (2005) Anticipatory activity in primary motor cortex codes memorized
movement sequences. Neuron 45:967–973.

Luria AR (1966) Higher cortical functions in man. New York: Basic Books.

Mai JK, Majtanik M, Paxinos G (2016) Atlas of the human brain, 4th ed. London:
Academic Press.

Matelli M, Camarda R, Glickstein M, Rizzolatti G (1986) Afferent and efferent
projections of the inferior area 6 in the macaque monkey. J Comp Neurol 251:281–
298.

Muellbacher W, Ziemann U, Wissel J, Dang N, Kofler M, Facchini S, Boroojerdi B,
Poewe W, Hallett M, Ko M (2002) Early consolidation in human primary motor
cortex. Nature 415:640–644.

Oldfield RC (1971) The assessment and analysis of handedness: the Edinburgh

inventory. Neuropsychologia 9:97–113.

Orban P, Peigneux P, Lungu O, Albouy G, Breton E, Laberenne F, Benali H, Maquet P,

Doyon J (2010) The multifaceted nature of the relationship between performance

and brain activity in motor sequence learning. Neuroimage 49:694–702.

Pascual-Leone, A., & Torres, F. (1993). Plasticity of the sensorimotor cortex

representation of the reading finger in Braille readers. *Brain*, *116*, 39–52.

Pascual-Leone, A., Cammarota, A., Wassermann, E. M., Brasil-Neto, J. P., Cohen, L.

G., & Hallett, M. (1993). Modulation of motor cortical outputs to the reading hand

of braille readers. *Ann Neurol*, *34*, 33–37.

Pascual-Leone, A., Wassermann, E. M., Sadato, N., & Hallett, M. (1995). The role of

reading activity on the modulation of motor cortical outputs to the reading hand in

Braille readers. *Ann Neurol*, *38*(6), 910–915.

Penhune VB, Doyon J (2002) Dynamic cortical and subcortical networks in learning

and delayed recall of timed motor sequences. J Neurosci 22:1397–1406.

Petrides M, Pandya DN (1984) Projections to the frontal cortex from the posterior

parietal region in the rhesus monkey. J Comp Neurol 228:105–116.

Rauch SL, Whalen PJ, Savage CR, Curran T, Kendrick A, Brown HD, Bush G, Breiter

HC, Rosen BR (1997) Striatal recruitment during an implicit sequence learning

task as measured by functional magnetic resonance imaging. Hum Brain Mapp

5:124–132.

Riera JJ, Bosch J, Yamashita O, Kawashima R, Sadato N, Okada T, Ozaki T (2004)

fMRI activation maps based on the NN-ARx model. Neuroimage 23:680–697.

Rizzolatti G, Fogassi L, Gallese V (1997) Parietal cortex: from sight to action. Curr

Opin Neurobiol 7:562–567.

Sadato N, Ibañez V, Campbell G, Deiber MP, Le Bihan D, Hallett M, Ibanez V, Deiber

MP, Bihan L (1997) Frequency-dependent changes of regional cerebral blood flow

during finger movements: functional MRI compared to PET. J Cereb Blood Flow

Metab 17:670–679.

Sadato N, Ibanez V, Deiber M-PP, Campbell G, Leonardo M, Hallett M, Le Bihan D

(1996) Frequency-dependent changes of regional cerebral blood flow during finger

movements. J Cereb Blood Flow Metab 16:670–679.

Shmuelof L, Krakauer JW, Mazzoni P (2012) How is a motor skill learned? Change and

invariance at the levels of task success and trajectory control. J Neurophysiol

108:578–594.

Tanabe H, Kochiyama T, Hasegawa K, Amano H, Ogihara N (2014) Difference of brain

function between Homo neanderthalensis and Homo sapiens based on the

endocranial morphometry. In: The Anthropological Society of Nippon 68th Annual

Meeting. Hamamatsu.

van Albada S, Robinson P (2007) Transformation of arbitrary distributions to the

normal distribution with application to EEG test-retest reliability. Journal of

Neuroscience Methods 161: 205–211.

Verstynen T, Diedrichsen J, Albert N, Aparicio P, Ivry RB (2005) Ipsilateral motor

cortex activity during unimanual hand movements relates to task complexity. J

Neurophysiol 93:1209–1222.

Walker MP, Brakefield T, Hobson JA (2003) Dissociable stages of human memory

consolidation and reconsolidation. Nature 425:8–12.

Walker MP, Brakefield T, Morgan A, Hobson JA, Stickgold R (2002) Practice with

sleep makes perfect: sleep-dependent motor skill learning. Neuron 35:205–211.

Wheaton LA, Hallett M (2007) Ideomotor apraxia: a review. J Neurol Sci 260:1–10.

Wheaton LA, Shibasaki H, Hallett M (2005) Temporal activation pattern of parietal and

premotor areas related to praxis movements. Clin Neurophysiol 116:1201–1212.

Wiestler T, Waters-Metenier S, Diedrichsen J (2014) Effector-independent motor

sequence representations exist in extrinsic and intrinsic reference frames. J

Neurosci 34:5054–5064.

Wise SP, Boussaoud D, Johnson PB, Caminiti R (1997) Premotor and parietal cortex : Corticocortical connectivity and combinatorial computations 1. Annu Rev Neurosci 20:25–42.

Wolpert DM, Ghahramani Z, Jordan MI (1995) An internal model for sensorimotor integration. Science 269:1880–1882.

Worsley KJ, Friston KJ (1995) Analysis of fMRI time-series revisited. Neuroimage 2:45–53.

Zuo XN, Ehmke R, Mennes M, Imperati D, Castellanos FX, Sporns O, Milham MP (2012) Network centrality in the human functional connectome. Cereb Cortex 22:1862–1875.

9. Figures
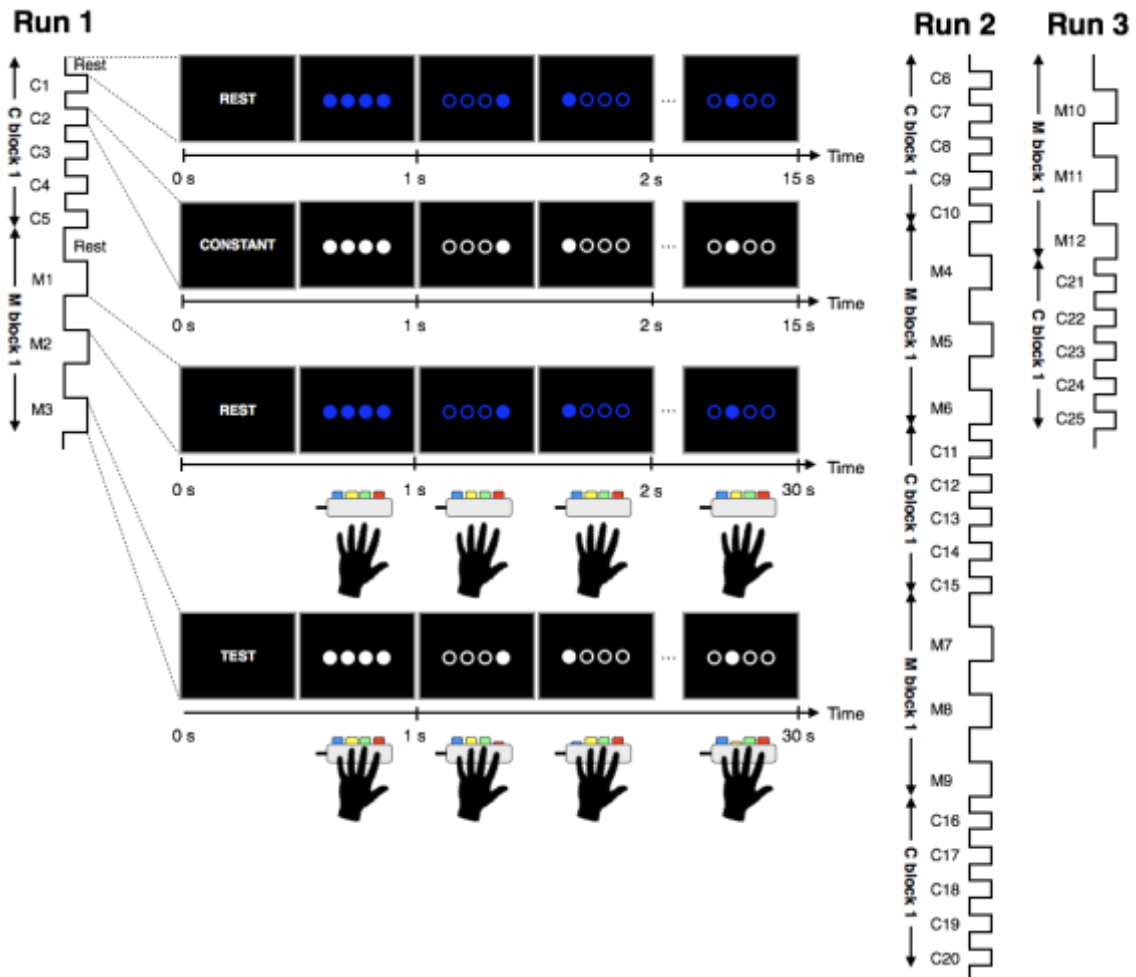
Figure 1. The block design of fMRI runs.

The task was consisted of 3 runs with total of 25 epochs of constant-speed mode (C1 to

C25) and 12 epochs of maximum mode (M1 to M12). On the screen, four blue circles

were aligned within an equally spaced horizontal array, corresponding to the left-hand

fingers through the spatial arrangement of the buttons. The duration of each epoch of C

block was 15 sec, and that during M block was 30 sec.
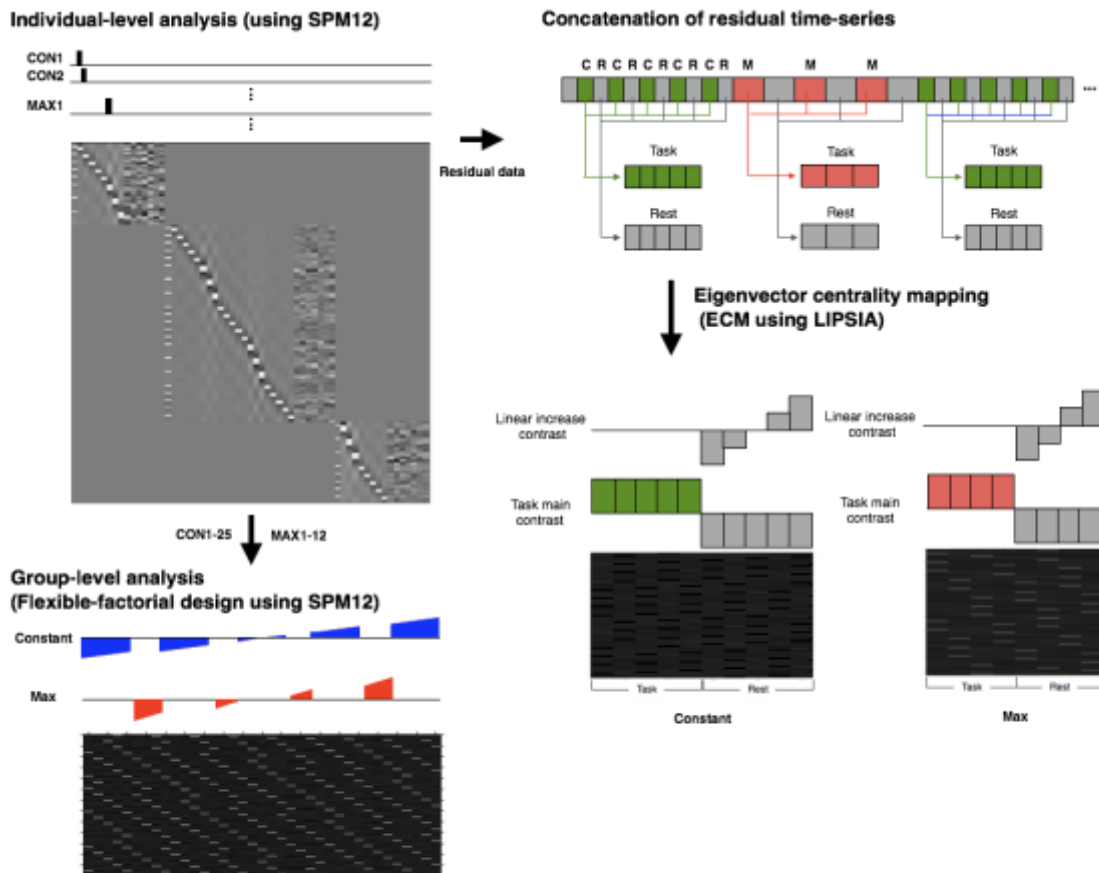
Figure 2 Statistical analysis with general linear model at individual level (top left). The

parameter estimates were incorporated into the group-level analysis with flexible

factorial design (bottom left). Concatenation of the residual time-series data for ECM

analysis (right).
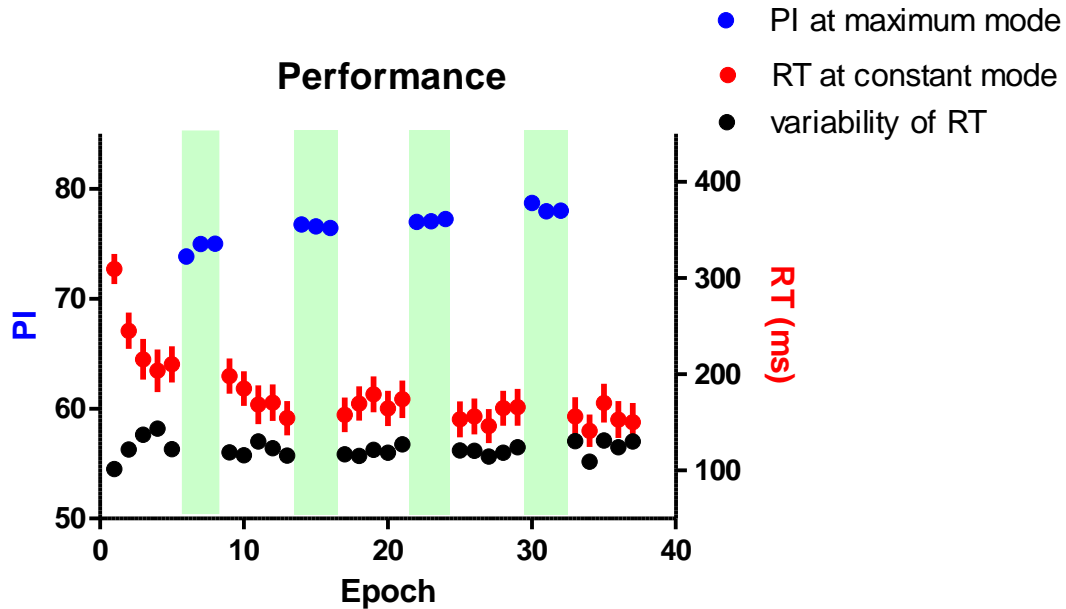
Figure 3. Performance in maximum mode (green shed) and constant mode. The performance of maximum mode was measured by performance index (PI, blue filled circle).   Reaction time (RT, ms, red filled circle) from the visual cue and the tap during constant mode and their variability regarding the standard deviation (black filled circle) are also plotted. Data points represent group means for each epoch, and error bars indicate the standard error of the mean.
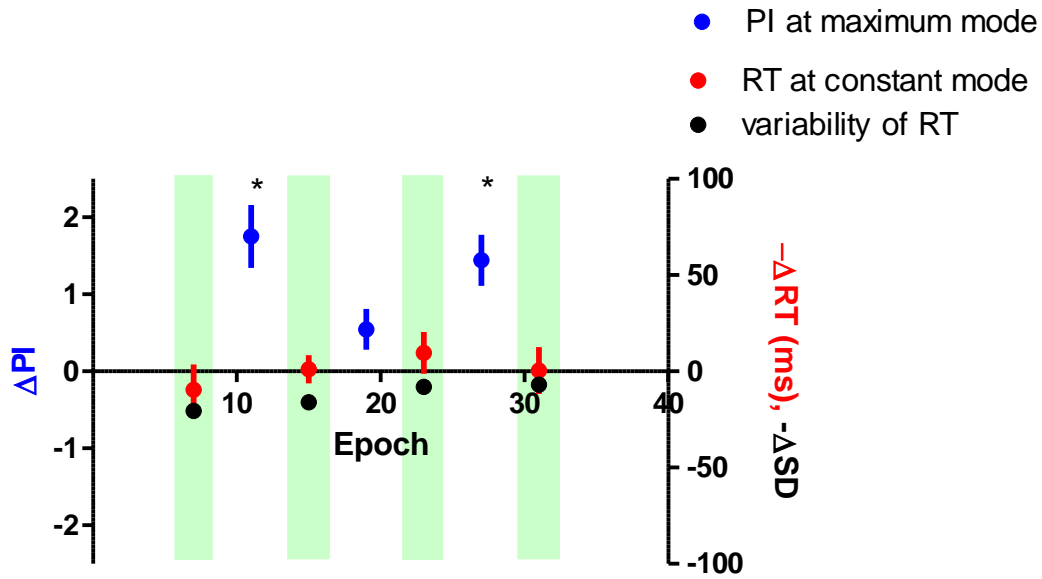
Figure 4.   Performance transfer. The change of PI from the last epoch of the preceding maximum mode block to that of the first epoch of the following maximum mode block (blue filled circle) was plotted between the consecutive maximum mode blocks. * P< 0.001. The change in RT (red filled circle) and variability of RT (black filled circle) in the consecutive constant blocks were plotted in the same format. Data points represent group means for each epoch, and error bars indicate the standard error of the mean.
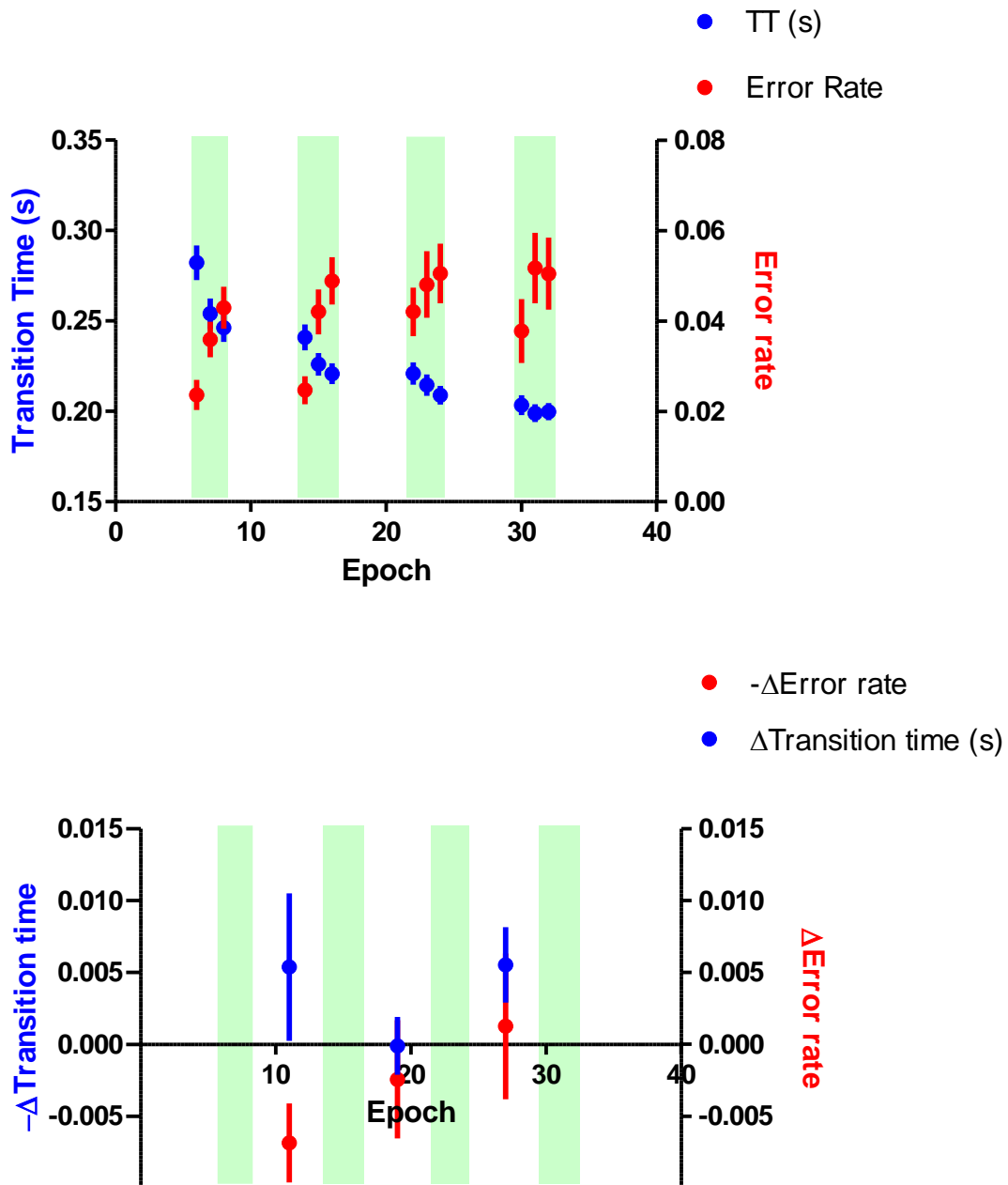
Figure 5. The performance of the maximum mode (top). The change of speed

(regarding transition time, TT, blue filled circle) and the error rate (red filled circle) are

plotted as group means for each epoch with an error bar of the standard error of the

mean. Learning transfer from the constant mode (bottom). The change of TT (blue filled

circle) and error rate (red filled circle) from the last epoch of the preceding maximum

mode block to that of the first epoch of the following maximum mode block were

plotted between the consecutive maximum mode blocks. Data points represent group

means for each epoch, and error bars indicate the standard error of mean.
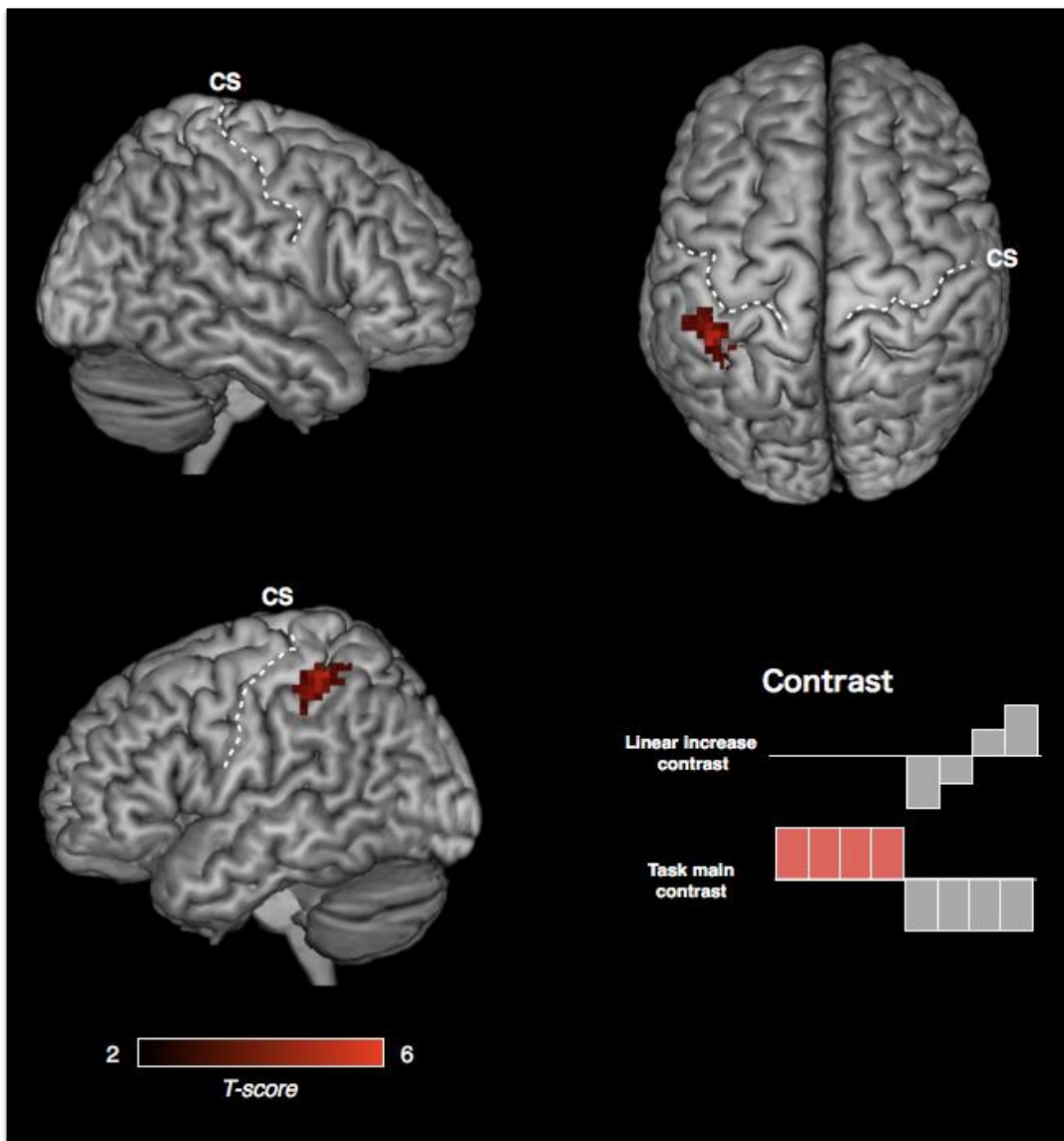
Figure 6. Motor engram generated by maximum mode training

Conjunction analysis of the linear increase of EC during rest epoch and the task related

increase of EC. P< 0.05 corrected at the cluster level, with height threshold Z > 3.09

(Friston et al. 1996). CS, central sulcus.
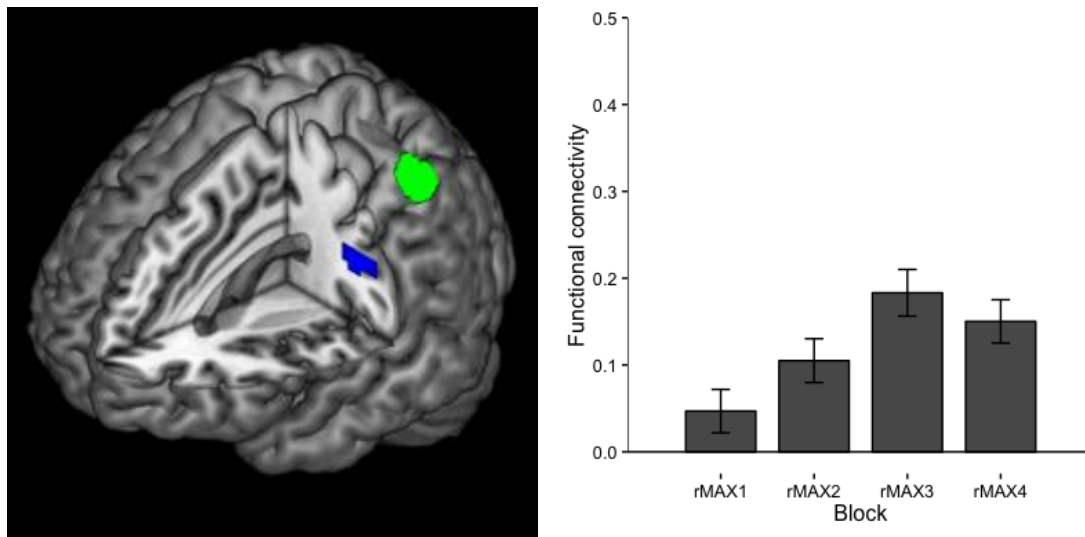
Figure 7. Learning related enhancement of the functional connectivity with the left aIPS

(seed, green) by maximum mode training (blue). P< 0.05 corrected at the cluster level,

with height threshold Z > 3.09 (Friston et al. 1996).
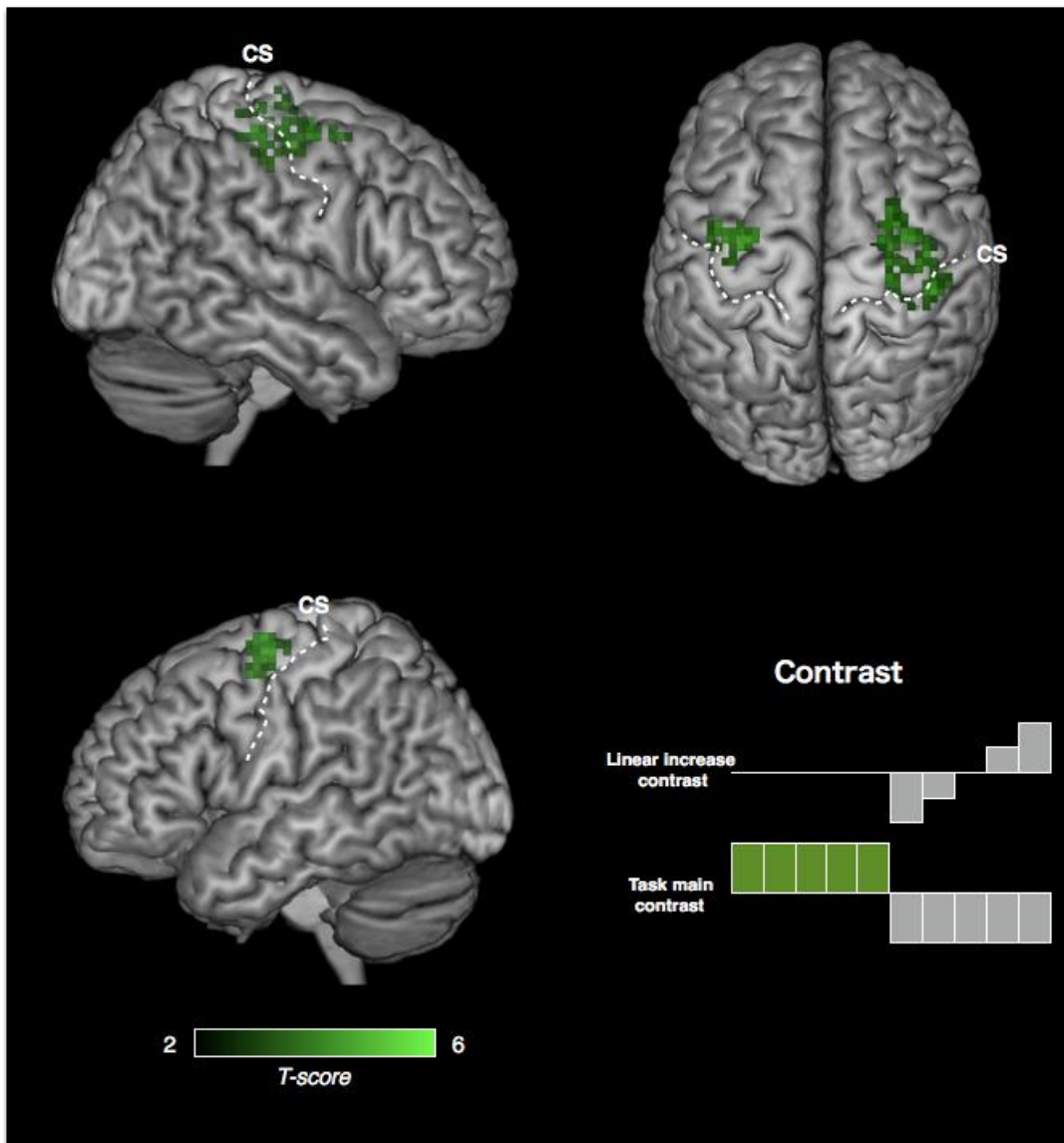
Figure 8. Motor engram generated by constant mode training

Conjunction analysis of the linear increase of EC during rest epoch and the task related

increase of EC. P< 0.05 corrected at the cluster level, with height threshold Z > 3.09

(Friston et al. 1996). CS, central sulcus.
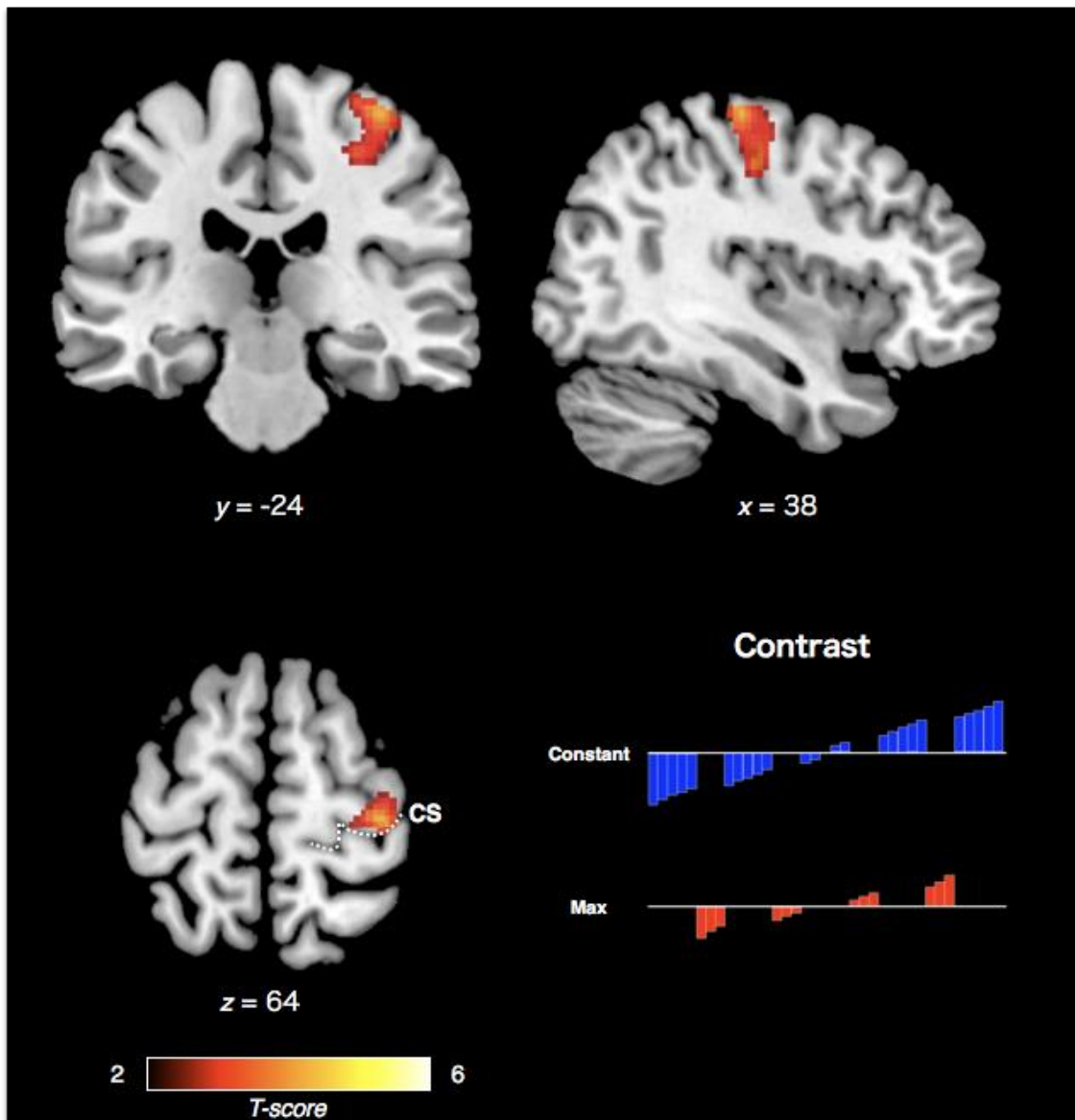
Figure 9. Task-related activity linearly increased by both constant and maximum modes.

The focus of activation on a pseudocolor fMRI superimposed on a high-resolution

anatomical MRI in the coronal (upper left), sagittal (upper right) and transaxial (lower

left) planes, sectioned at (38, -24, 64) corresponding to the primary motor cortex

(Brodmann area 4). Conjunction analysis of the linear increase of the task-related

activation of contant and maximum modes (lower right). P< 0.05 corrected at the cluster

level, with height threshold Z > 3.09 (Friston et al. 1996). CS, central sulcus.

10. Tables

Table 1. Brain areas showing both the learning-related increase in rest-state eigenvector centrality and the task-related increase in eigenvector centrality during maximum mode

Cluster size (mm^3)	p value	Anatomical location	Hem	Broadmann area	MNI Coordinates			Z value
					x	y	z	
528	1.42×10^{-7}	Intraparietal sulcus	L	40/7	-45	-42	57	5.00
		Inferior parietal lobule	L	40	-54	-33	51	3.65
		Inferior parietal lobule	L	40	-39	-36	51	4.15

Note. Statistical threshold was FEW corrected $p < .05$ at the cluster level with the height threshold of $Z > 3.09$. x, y, and z are stereotaxic coordinates (mm). *Hem*, Hemisphere; R, Right; L, Left.

Table 2. Brain areas showing both the learning-related increase in rest-state eigenvector centrality and the task-related increase in eigenvector centrality during constant mode

Cluster size (mm^3)	p value	Anatomical location	Hem	Broadmann area	MNI Coordinates			Z value
					x	y	z	
368	1.13×10^{-5}	Precentral gyrus	L	4	-36	-15	63	3.52
		Superior frontal sulcus	L	6	-33	-6	63	4.60
1064	1.39×10^{-12}	Postcentral gyrus	R	2	45	-27	60	4.29
		Precentral gyrus	R	4	42	-12	54	4.16
		Superior frontal sulcus	R	6	24	-9	51	4.34

Note. Statistical threshold was FEW corrected $p < .05$ at the cluster level with the height threshold of $Z > 3.09$. x, y, and z are stereotaxic coordinates (mm). *Hem*, Hemisphere; R, Right; L, Left.

Table 3.   Brain areas showing the linearly increase in task-related activations with the learning progress in both maximum and constant modes

Cluster size (mm^3)	p value	Anatomical location	Hem	Broadmann area	MNI Coordinates			Z value
					x	y	z	
3072	3.88×10^{-6}	Central sulcus	R	4/3	38	-24	64	4.56
		Precentral gyrus	R	4	38	-18	48	4.21

Note. Statistical threshold was FEW corrected $p < .05$ at the cluster level with the height threshold of $Z > 3.09$. x, y, and z are stereotaxic coordinates (mm). *Hem*, Hemisphere; R, Right; L, Left.